Supporting Information

Integrated leather-based fluid transport wearable sweat device for electrolyte balance monitoring

Tong Zhou,†[a] Shi Hu,†[a] Wenhui Ji,†[a] Yunqing Liu,[a] Rui Zhang,[a] Huanzhuan Liu,[a] Feng Wang,[a] Jingyu Zhu,[a] Chao Tao,[b] Baoli Zha,[a] Jiansheng Wu,*[a] Fengwei Huo[a]

[a.]Key Laboratory of Flexible Electronics (KLOFE), School of Flexible Electronics (Future Technologies), Institute of Advanced Materials (IAM), Nanjing Tech University, 30 South Puzhu Road, Nanjing 211816, China

[b.]Department of Neurosurgery, The First Affiliated Hospital of Nanjing Medical University, 300 Guangzhou Road, Nanjing 210029, China

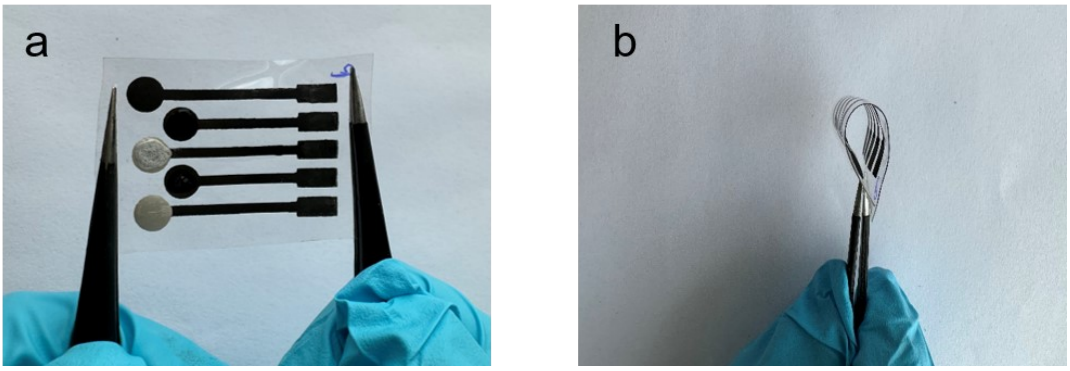

Figure S1 Optical pictures of a flexible sweat biosensor.

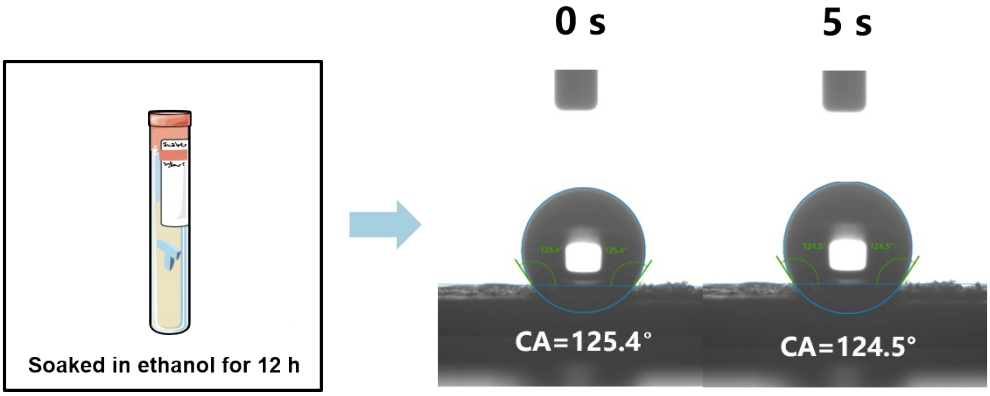

Figure S2 CA of leather after being immersed in ethanol for 12 hours.

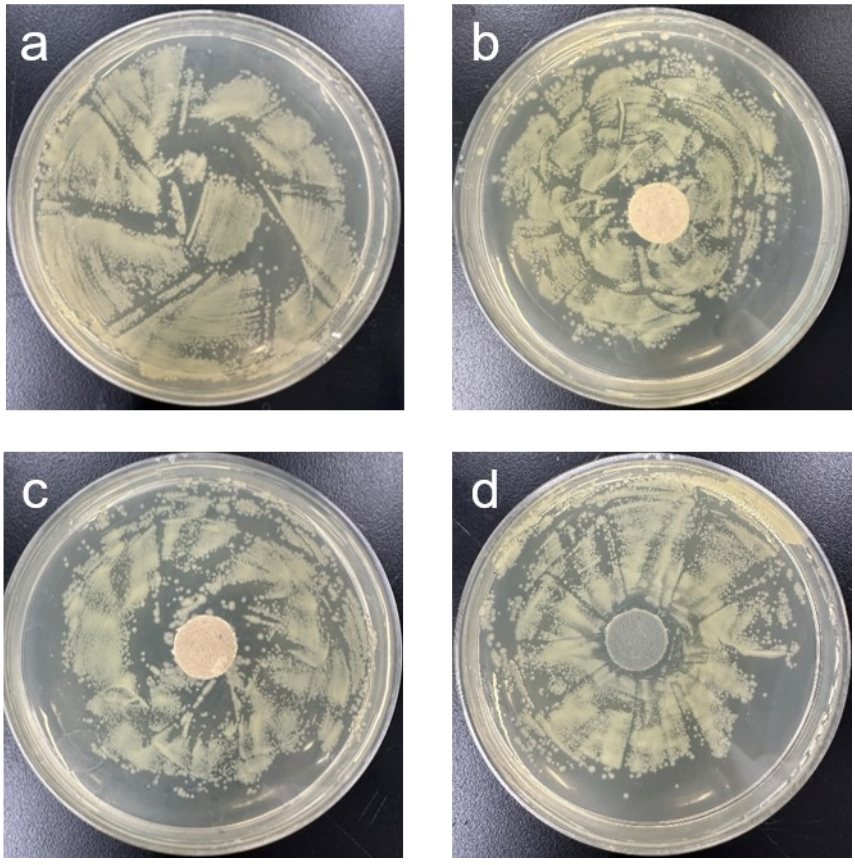

Figure S3 Antimicrobial effect of different treatments of leather. (a) Blank control for *E. coli*. **(b)** Inoculation of *E. coli* after soaking leather in pure water. **(c)** Inoculation of *E. coli* after ethanol-soaked leather. **(d)** Inoculation of *E. coli* after ethanol soaking followed by continued soaking of leather with sodium dodecyl sulfate.

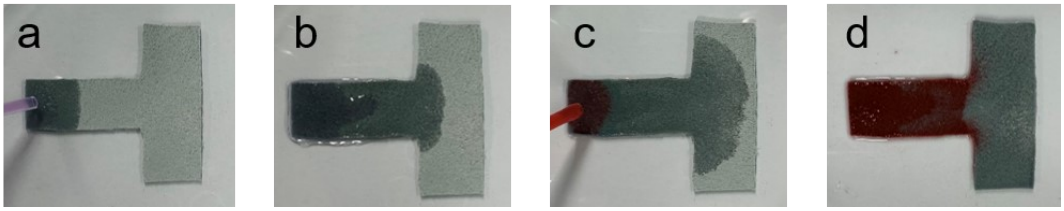

Figure S4 (a-d) Pigment flow from the collection zone to the evaporation zone of the leather.

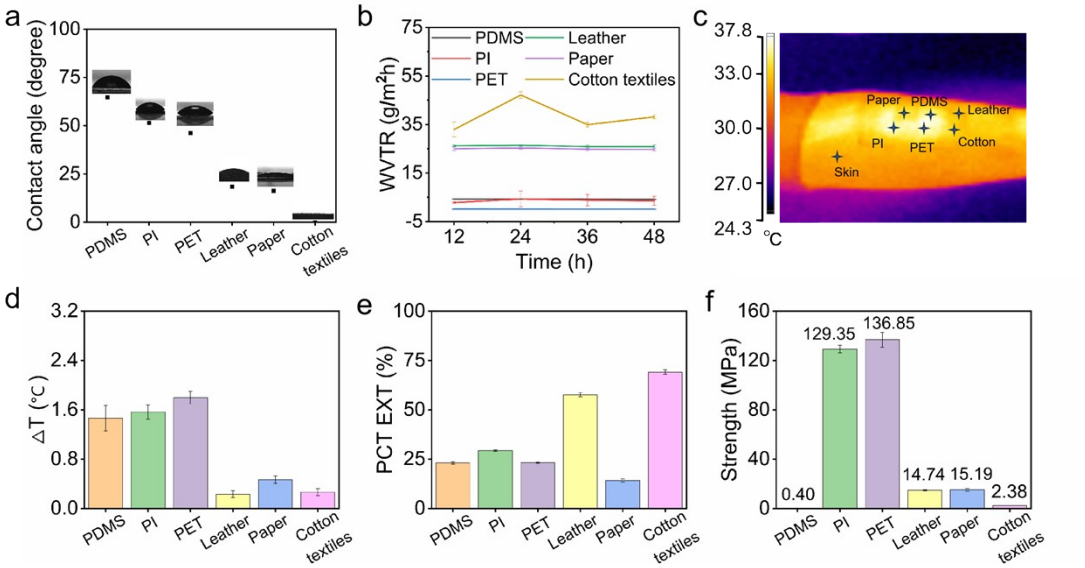

Figure S5 Hydrophilic, breathable and mechanical properties of different materials. (a) CA of different flexible substrates. (b) Comparison of WVTR between the leather and other flexible substrates. (n = 3) (c) Infrared photos of various substrates on the skin after a period of exercise. (d) Central temperature variation of skin-worn sensors as compared to the temperature of the surrounding naked skin after exercise. (n = 3) (e) Comparison of percentage extension of different substrate materials. (n = 3) (f) Comparison of tensile strength of different substrate materials (n = 3).

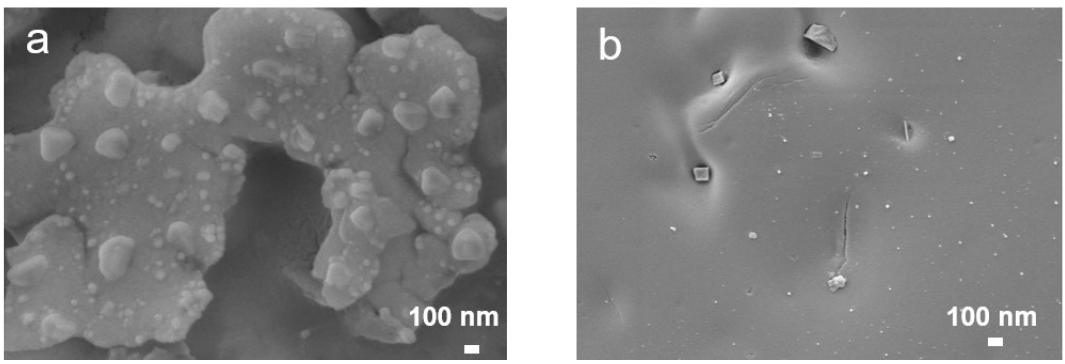

Figure S6 (a) SEM images of Ag and **(b)** PVB.

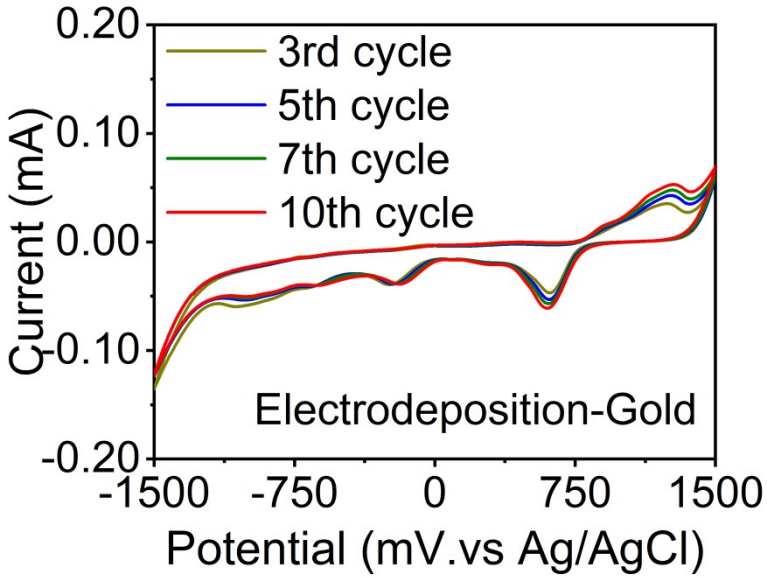

Figure S7 Cyclic voltammetry of electrodeposited gold nanoparticles (AuNPs).

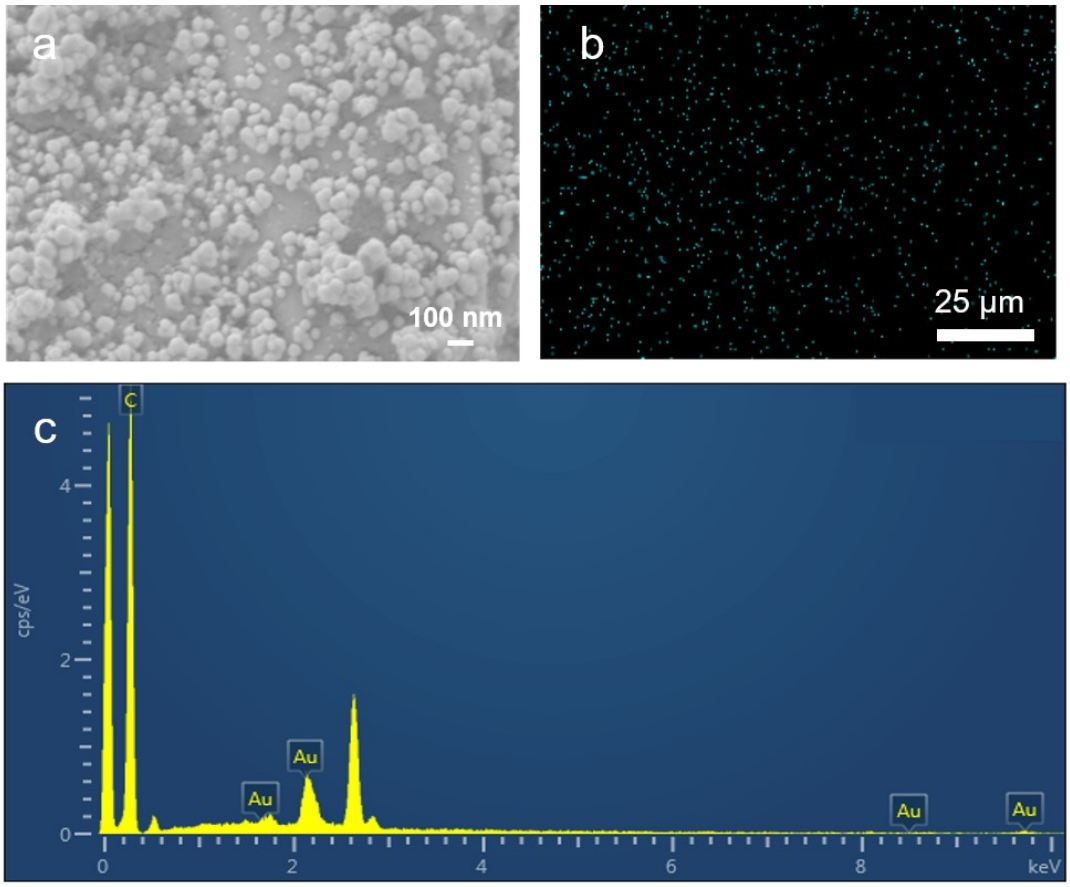

Figure S8 Characterization of AuNPs. (a) SEM image of AuNPs. **(b)** EDS spectra of AuNPs. **(c)** EDS spectra images of sensors.

The pH sensor is prepared using PANI via CV on a carbon electrode. As depicted in Figure S7b, a three-dimensional network structure is distributed on the carbon electrode. Additionally, the infrared characteristic spectra of PANI show two typical characteristic peaks located at 1592 cm^{-1} and 1520 cm^{-1}, corresponding to the C=N and C=C stretching vibrations of the quinone ring and the benzene ring. The peak at 1408 cm^{-1} is attributed to the C−N stretching of the benzene ring unit, while the peak near 1149 cm^{-1} can be explained by the C=N stretching vibration of the doped quinone unit. The broad peak near 3323 cm^{-1} is attributed to the N−H stretching or −OH groups, and the peak at 816 cm^{-1} is related to the C−H stretching vibration.

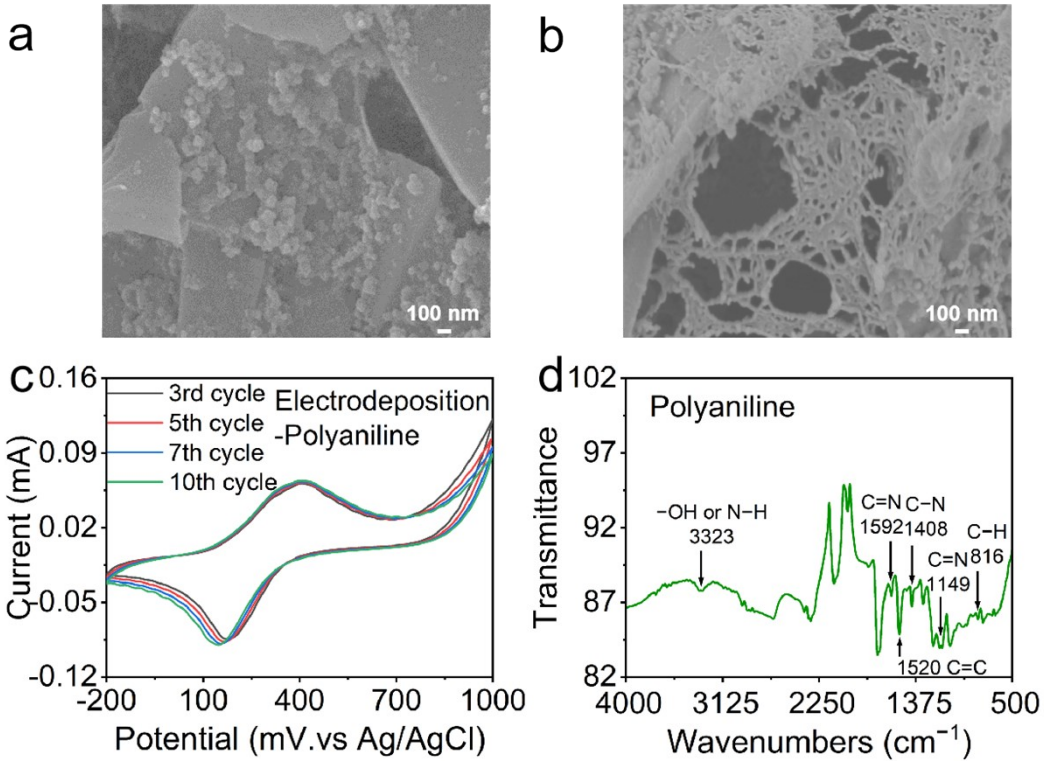

Figure S9 Characterization of pH sensors. (a) SEM image of carbon electrode**. (b)** SEM image of polyaniline. **(c)** Cyclic voltammetry of polyaniline. **(d)** Infrared absorption spectra of polyaniline.

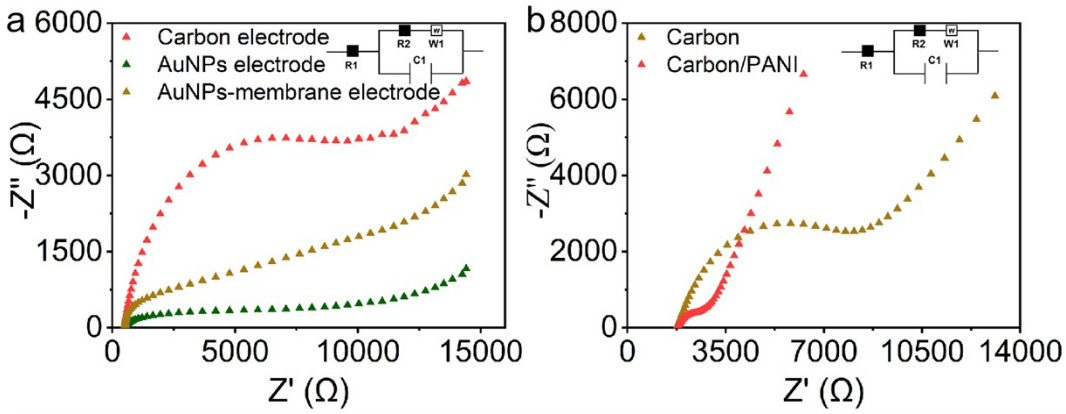

Figure S10 Electrochemical impedance spectroscopy (EIS) of different modified electrodes. (a) EIS comparison of carbon electrode, carbon electrode/AuNPs, and carbon electrode/AuNPs/membrane. **(b)** EIS comparison of carbon electrode and carbon electrode/PANI.

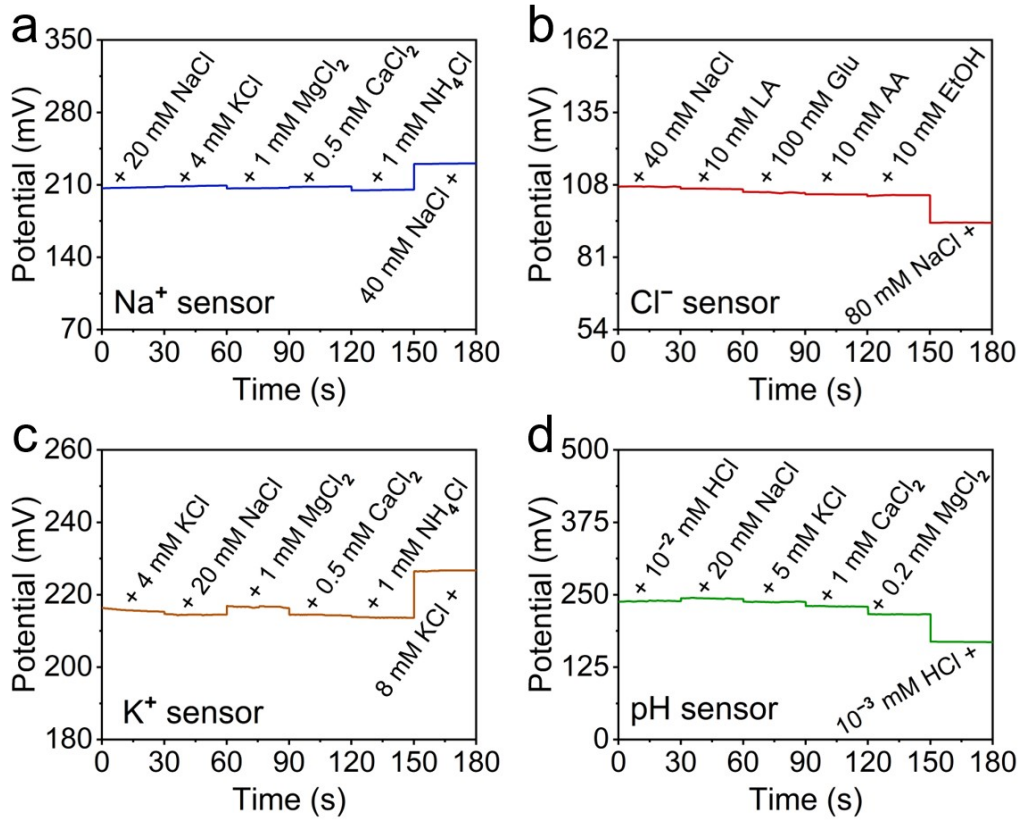

Figure S11 Selective testing. (a) Potential changes after adding KCl, $MgCl_2$, $CaCl_2$, NH_4Cl to the Na^+ sensor. **(b)** Potential changes after adding lactic acid (LA), glucose (Glu), ascorbic acid (AA), ethyl alcohol (EtOH) to the Cl^- sensor. **(c)** Potential changes after adding NaCl, $MgCl_2$, $CaCl_2$, NH_4Cl to the K^+ sensor. **(d)** Potential changes after adding NaCl, KCl, $MgCl_2$, $CaCl_2$ to the pH sensor.

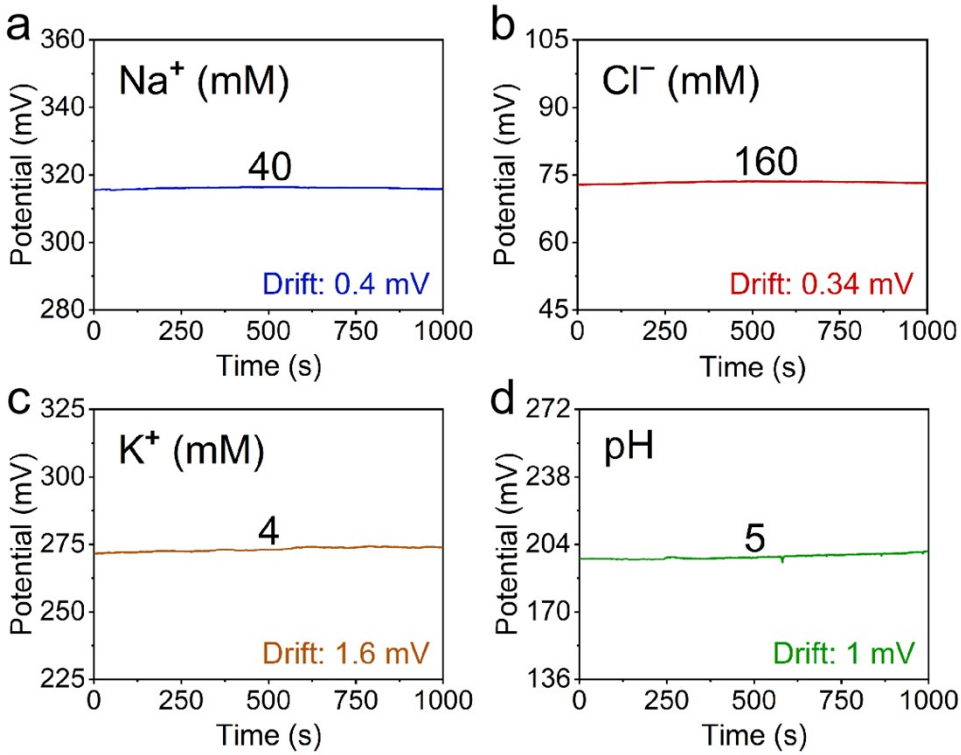

Figure S12 Stability tests. (a) Change in potential over 1000 seconds when the Na^+ concentration is 40 mM. **(b)** Change in potential over 1000 seconds when the Cl^- concentration is 160 mM. **(c)** Change in potential over 1000 seconds when the K^+ concentration is 4 mM. **(d)** Change in potential over 1000 seconds when the pH is 5.

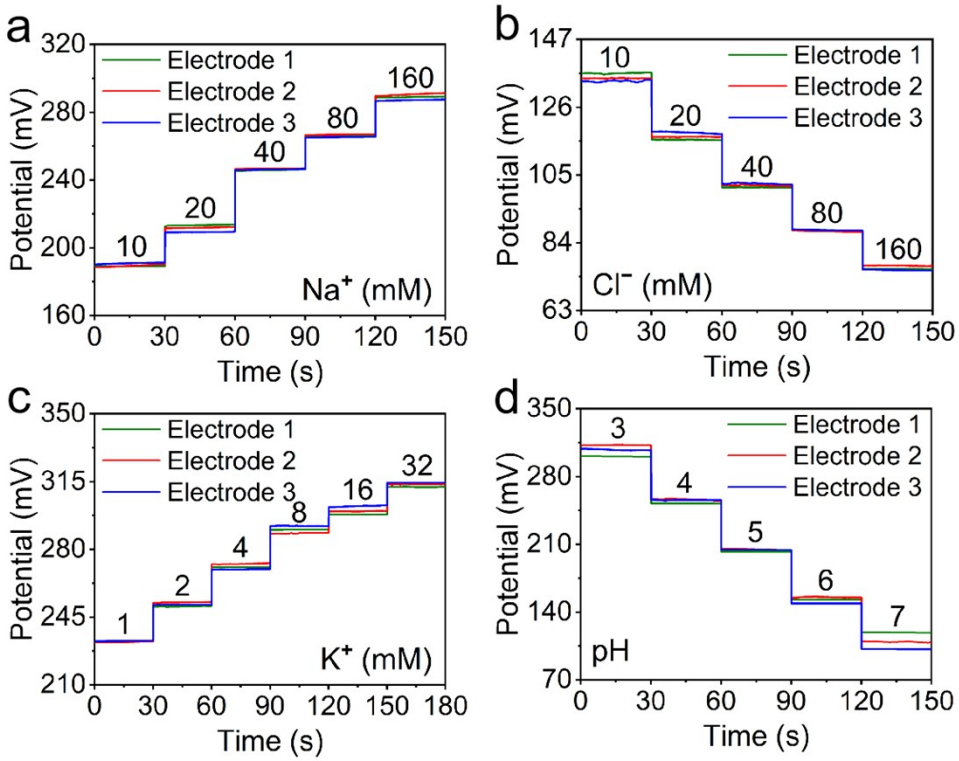

Figure S13 Repeatability testing. (a) Potential response of three Na^+ sensors in 10-160 mM solutions. **(b)** Potential response of three Cl^- sensors in 10-160 mM solutions. **(c)** Potential response of three K^+ sensors in 1-32 mM solutions. **(d)** Potential response of three pH sensors in pH=3-7.

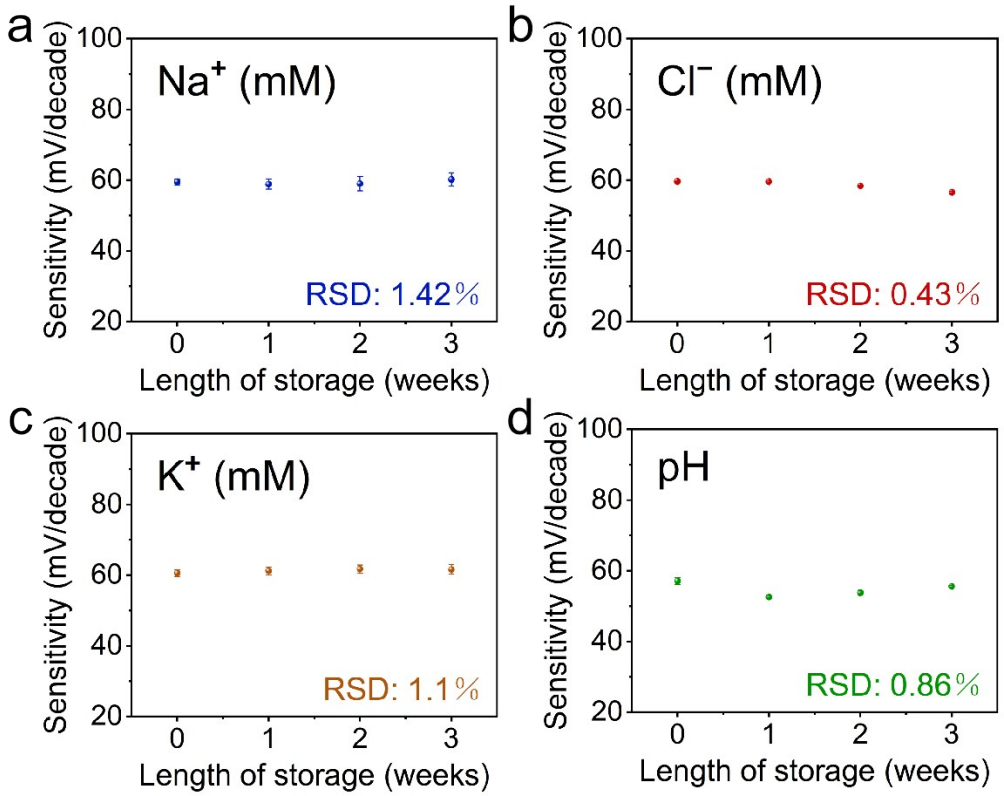

Figure S14 Long-term storage performance. (a) Sensitivity of Na^+ sensor stores for three weeks. **(b)** Sensitivity of Cl^- sensor stores for three weeks. **(c)** Sensitivity of K^+ sensor stores for three weeks. **(d)** Sensitivity of pH sensor stores for three weeks.

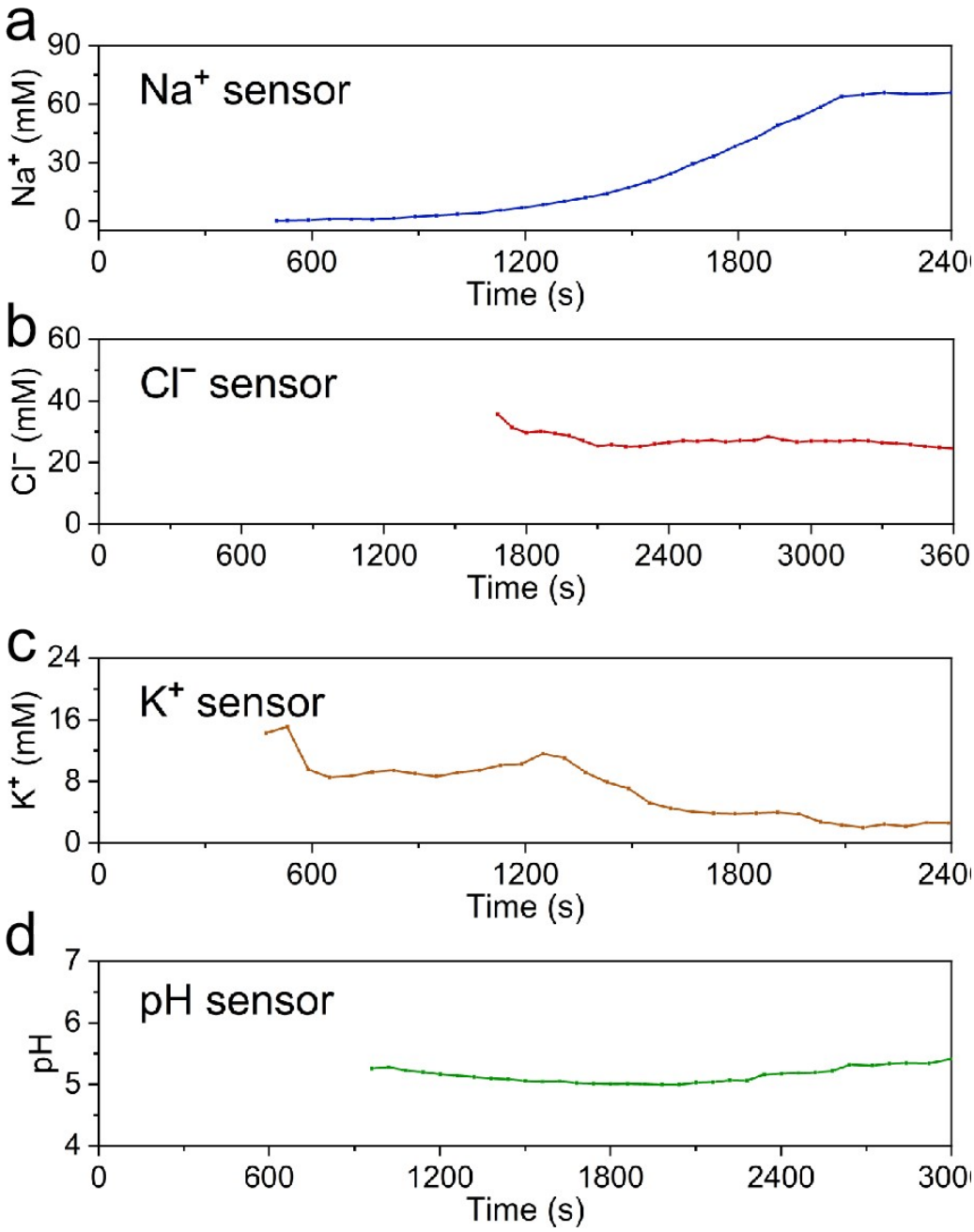

Figure S15 The electrochemical workstation tests the performance of sensors during exercise. (a) Potential trend of Na^+ sensors. **(b)** Potential trend of Cl^- sensors. **(c)** Potential trend of K^+ sensors. **(d)** Potential trend of pH sensors.

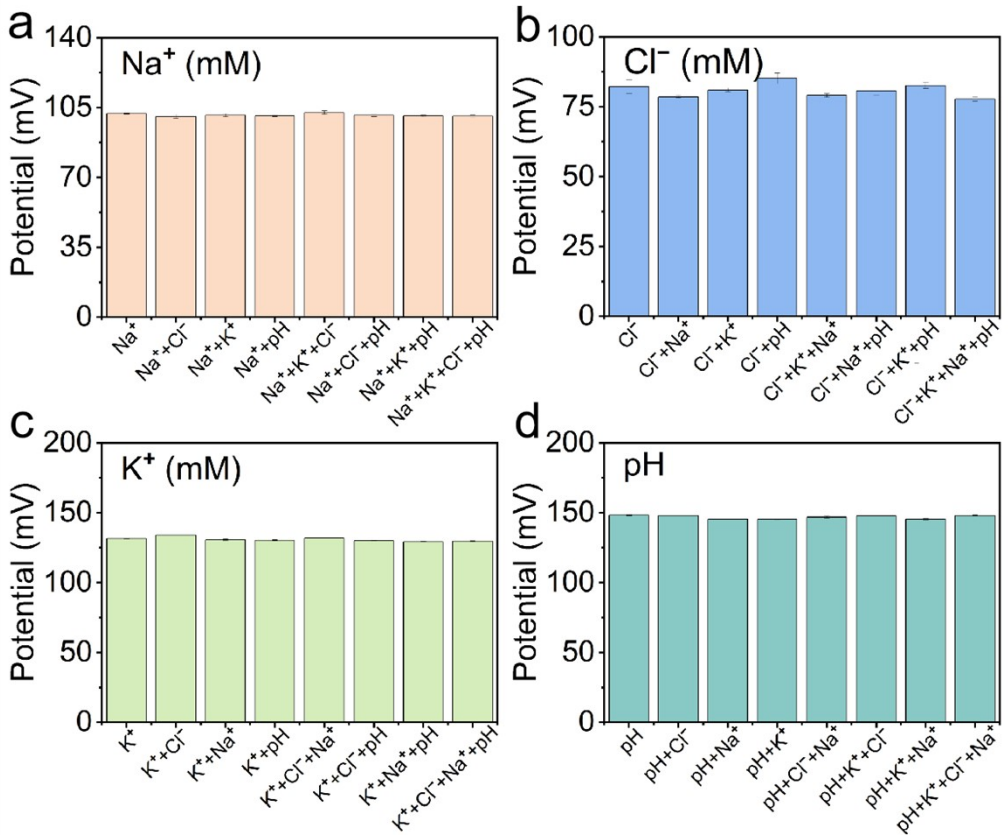

Figure S16 Ion crosstalk test. (a) Potential changes in single, two, three and four channel tests for Na^+ sensor**. (b)** Potential changes in single, two, three and four channel tests for Cl^- sensor**. (c)** Potential changes in single, two, three and four channel tests for K^+ sensor**. (d)** Potential changes in single, two, three and four channel tests for pH sensor**.**

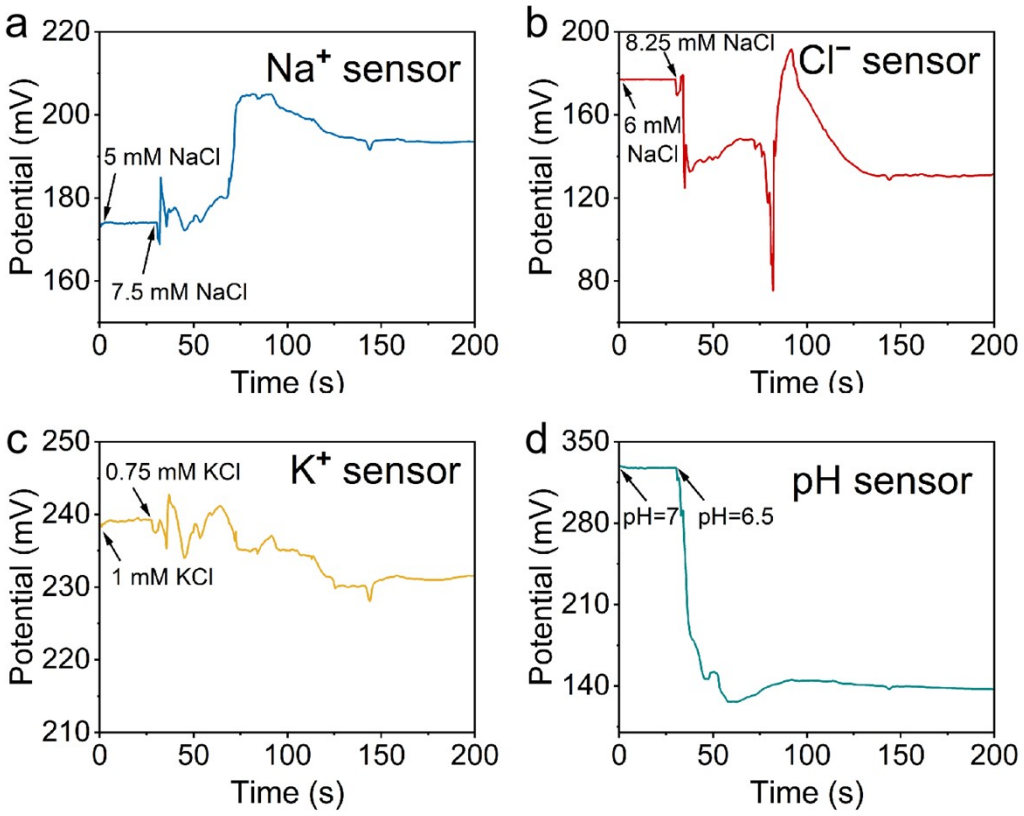

Figure S17 Characterization of sensor response time. (a) A change in potential is obtained by the addition of 7.5 mM Na^+ to 5 mM Na^+ solution. **(b)** A change in potential is obtained by the addition of 8.25 mM Cl^- to 6 mM Cl^- solution. **(c)** A change in potential is obtained by the addition of 0.75 mM K^+ to 1 mM K^+ solution. **(d)** A change in potential is obtained by the addition of pH=6.5 to pH=7.

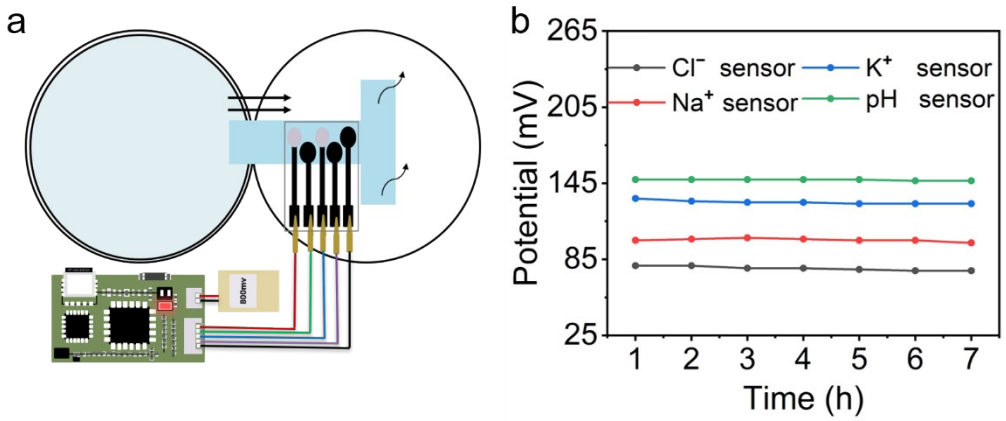

Figure S18 Long-term stability testing of the fully integrated wearable device. (a) Schematic diagram of the device. **(b)** Potential changes of the sensor under standard solution for 7 hours.

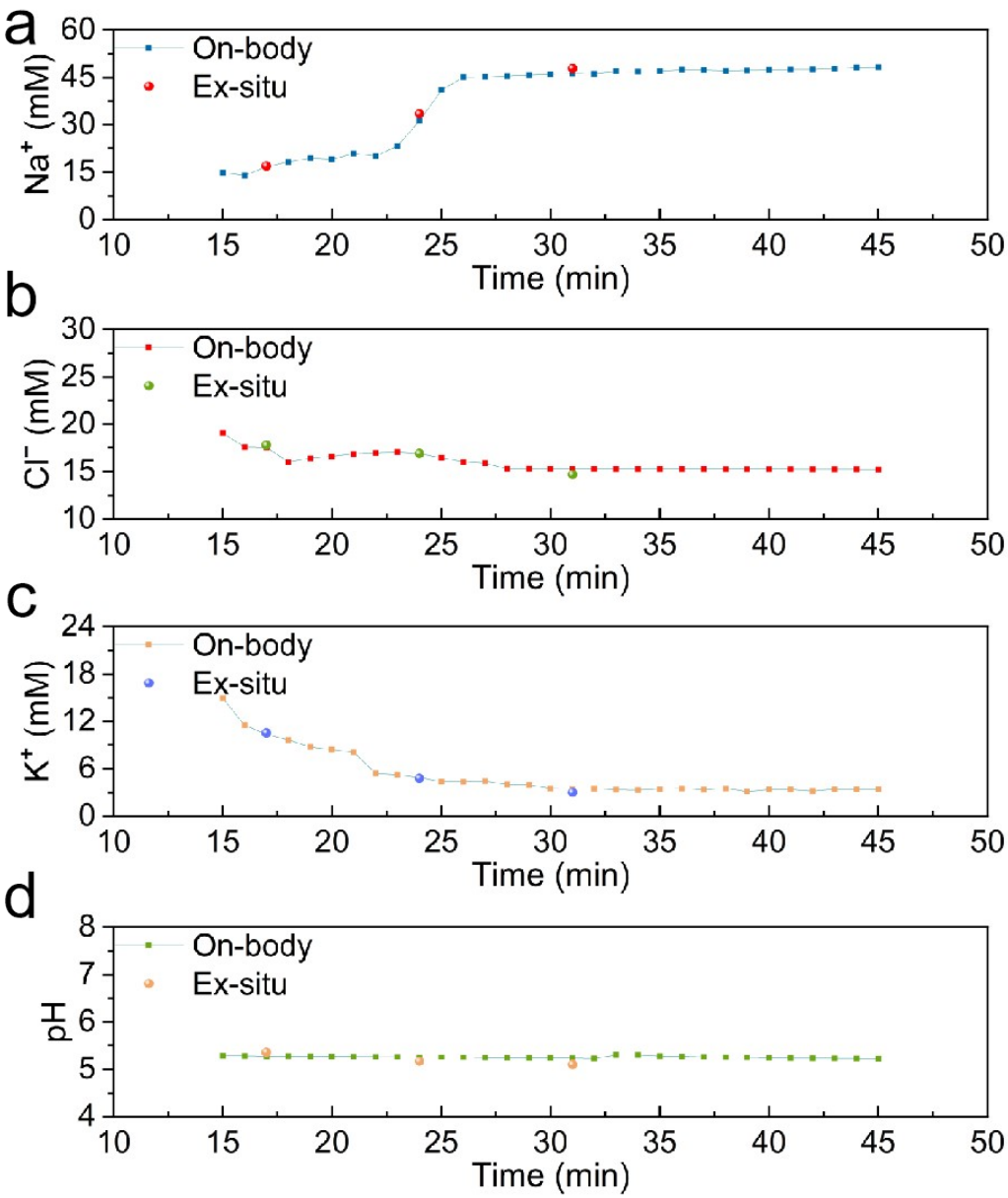

Figure S19 Comparison of results from in vitro and sensor testing of sweat. (a) Na^+ concentrations in sweat samples were determined using the standard method of ICP-OES and Na^+ sensor. **(b)** Concentration of Cl^- in sweat samples can be determined by using $AgNO_3$ titration and Cl^- sensor. **(c)** K^+ concentrations in sweat samples were determined using the standard method of ICP-OES and K^+ sensor. **(d)** Concentration of pH in sweat samples can be determined by using pH meter and pH sensor.